

DISCOVERY OF A NUCLEAR GAS BAR FEEDING THE ACTIVE NUCLEUS IN CIRCINUS¹R. MAIOLINO², A. ALONSO-HERRERO³, S. ANDERS⁴, A. QUILLEN³, M.J. RIEKE³, G.H. RIEKE³,
L.E. TACCONI-GARMAN⁴

ABSTRACT

We report the discovery of gas inflow motions towards the active nucleus of the Circinus galaxy caused by the non-axisymmetric potential of a nuclear gas bar. Evidence for dust associated with the bar comes from the HST/NICMOS $H - K$ color map, whereas the streaming motions along the gas bar are seen in the velocity field of the $\text{H}_2\text{S}(1)(1-0)$ emission line. The gas bar is about 100 pc long with a visual extinction in excess of 10 mag. Indication for the gaseous nature of this bar comes from the lack of a stellar counterpart even in the K band where the extinction is greatly reduced.

We also use the NICMOS emission line images ($\text{Pa}\alpha$, $[\text{Si VI}]$, and $[\text{Fe II}]$) to study the innermost region of the ionization cones and the nuclear star forming activity. We discuss the possible relationship of these components with the gaseous bar.

Subject headings: Galaxies: individual: Circinus – galaxies: nuclei – galaxies: active – galaxies: Seyfert – galaxies: kinematics and dynamics – infrared: galaxies

1. INTRODUCTION

Active galactic nuclei (AGNs) are thought to be powered by an accreting supermassive black hole ($M_{\text{BH}} \approx 10^6 - 10^{10} M_{\odot}$). The required accretion rate ranges from $10^{-2} - 10^{-1} M_{\odot} \text{yr}^{-1}$ (Seyfert nuclei) up to $10 - 100 M_{\odot} \text{yr}^{-1}$ (QSOs). Although the gas content of host galaxies is generally enough to fuel AGNs over the Hubble time, the mechanism responsible for transporting gas from the kpc scale into the nuclear region is still unclear. Indeed, the galactic gas must lose about 99.9% of its angular momentum before reaching the central few parsecs, where viscosity can be effective. The required accretion rates are lower in Seyfert galaxies than in QSOs and the gas inflow requirements from the host galaxy are relaxed. However, because of the large number of Seyfert galaxies ($\sim 10\%$) in the local Universe and the even larger fraction of AGNs at high redshifts (Ho et al. 1997, Maiolino & Rieke 1995, Hasinger et al. 1998, Miyaji et al. 1999), some mechanism for transporting gas from the circumnuclear 100 pc into the central parsec is still required to maintain the activity of these nuclei. Also, the accumulation of large quantities of gas in the innermost region of Seyfert nuclei is inferred from the observation that most of them are obscured by gaseous column densities in excess of 10^{24}cm^{-2} within the central 10 pc (Risaliti et al. 1999) and from the detection of maser emission within the nuclear few parsecs (Greenhill et al. 1997a, 1997b, 1998b, Greenhill & Gwinn 1997, Miyoshi et al. 1995).

Non-axisymmetric gravitational potentials are thought to be an efficient mechanism for transporting gas from the host galaxy into the central region (Athanasoula 1992, Helfer & Blitz 1995, Laine et al. 1999, Hernquist 1989, Quillen et al. 1995, Regan et al. 1997, Shlosman et al. 1990, Maiolino et al. 1999a). However, within the cen-

tral few hundred parsecs large scale disturbances have little effect in removing angular momentum from the gas, since on these scales the gravitational field is dominated by the central region of the bulge that is axially symmetric. Nested, secondary stellar bars have been observed in several barred system (Jungwiert et al. 1997, Friedli et al. 1996, Wozniak et al. 1995). These secondary bars are relatively small (a few 100 pc long) and could be responsible for transporting gas into the nuclear region to feed a black hole. Indeed, the fraction of Seyfert nuclei among the 40 double-barred systems known so far is about 1/3 to be compared to the fraction of Seyferts among all galaxies that is about 1/10 (Friedli 1999). Alternatively, Shlosman et al. (1989), Wada & Habe (1992) and Heller & Shlosman (1994) proposed that if the mass of gas gathered into the central region exceeds about 10% of the dynamical mass then the gaseous disk develops gravitational instabilities and forms a gaseous bar, which can drive gas further into the nuclear region. Indeed, there is evidence in several Seyfert nuclei for concentrations of gas whose mass approaches the dynamical mass (Meixner et al. 1990, Henkel et al. 1991, Risaliti et al. 1999), therefore gaseous bars are expected to form and to provide a mechanisms for the fuelling of the nuclear region. However, neither of these mechanisms appear to operate in the majority of Seyfert galaxies.

Understanding the mechanism responsible for the fuelling of active galaxies is also relevant to other issues. The dense gas funneled into the central region is photoionized by UV radiation from the nuclear source and/or is shock excited by the interaction with radio jets. Also, the large mass of gas driven into the central region and the perturbations due to the fuelling mechanism are expected to boost the star forming activity in the central region. There-

¹Based on observations with the NASA/ESA Hubble Space Telescope (obtained at the Space Telescope Science Institute, which is operated by the Association of Universities for Research in Astronomy, Inc. under NASA contract No. NAS5-26555) and with the Anglo-Australian Telescope (Siding Spring, Australia).

²Osservatorio Astrofisico di Arcetri, L.go E. Fermi 5, I-50125, Firenze, Italy

³Steward Observatory, The University of Arizona, 933 N. Cherry Ave., Tucson, AZ 85721

⁴Max-Planck-Institut für Extraterrestrische Physik, Postfach 1603, D-85740, Garching, Germany

fore, the fuelling mechanism of AGNs is likely to play a key role in the connection between starbursts and AGNs (Gonzalez-Delgado et al. 1998, Maiolino et al. 1997).

The Circinus galaxy is a nearby (4 Mpc), edge-on (incl. $\sim 65^\circ$), Sb-d system that is seen through a low interstellar extinction window near the Galactic plane ($A_V = 1.5$ mag, Freeman et al. 1977). The nuclear optical line ratios (Oliva et al. 1994) are typical of a Seyfert 2 galaxy. This classification is supported by the detection of intense coronal lines (Oliva et al. 1994, Moorwood et al. 1996), the discovery of an intense X-ray iron 6.4 keV line (Matt et al. 1996), rapid variation of the powerful H_2O maser emission (Greenhill et al. 1997c) and a prominent ionization cone in the $[\text{OIII}]\lambda 5007$ maps (Marconi et al. 1994a) with filamentary supersonic outflows (Veilleux & Bland-Hawthorn 1997). The detection of an X-ray excess above 30 keV reveals that the central engine is heavily obscured by a gaseous column density $N_{\text{H}} = 4 \times 10^{24} \text{cm}^{-2}$ along our line of sight (Matt et al. 1999). Large amounts of molecular gas in the central region of this galaxy have been inferred also from CO observations (Aalto et al. 1995, Elmouttie et al. 1998a, Curran et al. 1998, Johansson et al. 1991) and from the detection of a nuclear maser disk (Greenhill et al. 1998). $\text{H}\alpha$ and $[\text{SII}]$ narrow band images (Marconi et al. 1994a) have revealed a star forming ring at a radius of $\sim 10'' = 200 \text{pc}$, while Maiolino et al. (1998) have found evidence for a young stellar population in the central 10–100 pc with typical ages of the order of 10^8 yr. As a consequence, Circinus is an excellent candidate to search for a gaseous bar that might be feeding both the black hole and the star forming activity in the central region.

In this paper we present high angular resolution near infrared HST images and integral field spectra of the central region of the Circinus galaxy that reveal the presence of a small nuclear gaseous bar and show evidence for streaming motions of the gas along the bar.

2. OBSERVATIONS AND DATA REDUCTION

2.1. NICMOS observations

HST/NICMOS observations of Circinus were obtained during two different orbits on March 16 and October 16 1998 using the NIC2 and NIC3 cameras. In Table 1 we give the log of the NICMOS observations. Column (1) lists the NICMOS camera; column (2), the filter; column (3), the corresponding ground-based broad-band filter, emission line or adjacent continuum; column (4), the total integration time in seconds; and column (5), the original orientation of the images. The observations were taken in a spiral dither with a 5.5 pixel spacing between each of four positions. The plate scales for cameras NIC2 and NIC3 are $0.076''/\text{pixel}$ and $0.204''/\text{pixel}$ respectively.

The reduction of the NICMOS images used routines from the package NicRed (McLeod 1997). A master dark image was produced by combining between 10 and 20 darks for a given sample sequence after the subtraction of the first readout. The darks were taken from other programs carried out close in time. When possible we also generated our own flatfield images from on-orbit data. The flatfields used for the NIC3 narrow-band images were obtained as part of the camera 3 campaign in January 1998 and were kindly reduced and provided by Dr. Rodger Thompson. Only for the NIC2 F187N and NIC2 F190N

filters were in-flight flats not available, so thermal-vacuum flatfields were used instead. The data reduction was performed using the following steps: subtraction of the first readout; dark current subtraction on a read-by-read basis; correction for linearity and cosmic ray rejection (using the *fullfit* routine in NicRed); and flatfielding. The individual dithered galaxy images were registered to a common position using fractional pixel offsets and a cubic spline interpolation, and combined to produce the final image of each field. Since our NICMOS images were obtained after August 1997, no correction for the pedestal effect was necessary.

Prior to flux calibrating the images, the background needs to be subtracted from the images (this is important only for filters at wavelengths longer than $2\mu\text{m}$). Due to the large projected size of Circinus, the field of view of the NIC2 images is not large enough to allow measurements of the background on blank corners of the images, so we used background measurements taken during the Servicing Mission Observatory Verification (SMOV) program for the filter NIC2 F222M, and from our observations of the interacting galaxy Arp 299 for the NIC2 F160W filter. The NIC3 mosaics cover a larger field of view, and an estimate of the thermal background was obtained from the corners of the images. The flux calibration of the broad-band, on-line, and off-line images was performed using conversion factors (from ADU/s to mJy) from measurements of the standard star P330-E during SMOV.

NICMOS only provides continuum bands to the red of the emission lines. The extinction in the nuclear regions of Circinus is very high (even at infrared wavelengths), and a straight subtraction of the longer wavelength off-line image results in an overcorrection of the continuum at the wavelength of the emission line. To estimate the continuum at $1.644 \mu\text{m}$, $1.96 \mu\text{m}$, $2.122 \mu\text{m}$ and $1.87 \mu\text{m}$ for the NIC3 F164N, NIC3 F196N and NIC3 212N respectively, we fit the continuum between $1.66 \mu\text{m}$ and $1.90 \mu\text{m}$ using the NIC3 F166N and NIC3 F200N line-free images for the first two, and the NIC3 F200N and NIC3 F215N for the last image. The same procedure was followed to subtract the continuum at $1.87 \mu\text{m}$ for the NIC2 F187N image, using the NIC2 F160W and F222M images. The continuum fit is simply a linear regression of the flux as a function of the wavelength for each point in the image. An image at the required continuum wavelength is then constructed by extrapolation or interpolation of the corresponding fit. The extrapolated continuum is subtracted from the line+continuum images to produce the final $[\text{Fe II}]\lambda 1.644 \mu\text{m}$, $\text{Pa}\alpha$, $[\text{Si VI}]\lambda 1.96 \mu\text{m}$ and H_2 at $2.121 \mu\text{m}$ images. Due to the low surface brightness of the H_2 emission together with problems associated with the continuum subtraction, the resulting H_2 image had relatively low signal to noise, and therefore we used the H_2 map obtained with the 3D integral field spectrometer (see next section). Note however that when we rebinned the NICMOS H_2 image to the angular resolution of the 3D image, both images showed a similar morphology.

The images presented in this paper were taken during different orbits and hence have different orientations (see Table 1). Image rotation was removed by linear interpolation to the conventional orientation (north up, east to the left), both to provide the same orientation for all the images, and also to allow easy comparisons with previously

TABLE 1
LOG OF THE NICMOS OBSERVATIONS.

Camera	Filter	line/broad/cont	t_{exp}	orient
NIC2	F160W	H	192	94°
NIC2	F222M	K	192	94°
NIC2	F187N	$\text{Pa}\alpha$	384	-64°
NIC2	F190N	$\text{Pa}\alpha$ cont.	384	-64°
NIC3	F164N	$[\text{Fe II}]1.664 \mu\text{m}$	256	94°
NIC3	F166N	$[\text{Fe II}]$ cont.	256	94°
NIC3	F196N	$[\text{Si VI}]1.96 \mu\text{m}$	320	94°
NIC3	F200N	$[\text{Si VI}]$ cont.	320	94°
NIC3	F212N	$\text{H}_2 2.122 \mu\text{m}$	640	-64°
NIC3	F215N	H_2 cont.	640	-64°

published data.

2.2. 3D integral field spectroscopy

We observed the nuclear region of the Circinus galaxy on March 18th and 19th 1998 with the near infrared integral field spectrometer 3D (Weitzel et al. 1996), assisted by ROGUE, a first order adaptive optics system (Thatte et al. 1995), at the Anglo Australian Telescope. 3D slices the focal plane into 16 slits and disperses their light in wavelength; the spectrum of the slices is then imaged onto a NICMOS3 detector (256×256 pixels). The resulting “cube” provides simultaneous spectra of an area $6.4'' \times 6.4''$, as projected on the sky, divided into 16×16 pixels (i.e. $0.4''/\text{pix}$). Circinus was observed with a grism providing a spectral resolution of $\lambda/\Delta\lambda = 2100$ and covering the spectral range from $1.95 \mu\text{m}$ to $2.21 \mu\text{m}$. The average seeing for accepted observations, after tip-tilt correction, was about $0''.7 - 0''.8$. The (limited) field of view was not centered on the nucleus but was moved about 1 arcsec to the south-east so that it could include a dusty feature we were interested in. The total on source integration time was 20 minutes, split in twelve elementary integrations of 100 seconds. The elementary on-source integrations were interleaved with an equal number of acquisitions of sky frames for background subtraction. To avoid and control instrumental artifact we dithered the field of view around the region of interest so that each region of the source was observed by different regions of the slicer and of the detector. We observed a nearby O9 star to correct the atmospheric transmission features. Data reduction was performed as described in Weitzel et al. (1996) and Thatte et al. (1997). The subtraction of the continuum underneath the emission lines was performed with a first order fit to the continuum approximately $\pm 0.03 \mu\text{m}$ from each line.

3. THE NUCLEAR GAS BAR

3.1. Evidence for a radial dust lane

Fig. 1a shows a false color image of the central region of the Circinus galaxy ($26'' \times 29'' = 530 \times 590$ pc) obtained by combining HST images at $0.606 \mu\text{m}$ (WFPC2-F606W, blue), at $1.66 \mu\text{m}$ (NIC3-F166N, green), and at $2.0 \mu\text{m}$ (NIC3-F200N, red). The galactic disk is inclined by about 65° with respect to our line of sight (the South-East is the

near side of the disk) and the position angle of the major axis is about 25° . The image shows a spiral pattern with prominent dust lanes, consistent with the large amount of gas in this region as inferred from the CO millimetric data. Fig. 1b shows the H–K color map constructed with the NIC2-F160W (\sim H band) and NIC2-F222M (\sim K band) images.

The H–K color of the nucleus (identified with the $2 \mu\text{m}$ peak) is extremely red and in the F222M (\sim K band) image the nucleus dominates the emission within the central two arcseconds. As discussed in detail in Maiolino et al. (1998), the powerful K band emission is due to hot dust, heated by the active nucleus and located in a region smaller than 1.5 pc ($= 0''.07$ arcsec) in radius. In Fig. 1b we have subtracted a nuclear unresolved source using the NIC2 point spread function as modeled by the *TinyTim* software (Krist & Hook 1997). This subtraction allows study of the H–K color of the circumnuclear two arcseconds (although in the innermost arcsecond there are some residuals probably due to imperfect subtraction). The PSF subtraction does not affect the color map outside this inner region.

The H–K color of the circumnuclear region is still significantly redder than colors typical of stellar populations older than 10^7 yr: $(\text{H}-\text{K}) \approx 0.22$, as observed both in galaxies that do not suffer heavy extinction, and also as predicted by population models. Such off-nuclear red colors cannot be ascribed to hot dust emission in the K band, for the CO stellar bands at $2.29 \mu\text{m}$ do not appear diluted by non-stellar emission in these regions (Maiolino et al. 1998). In addition, the H–K color does not correspond with the $\text{Pa}\alpha$ and $\text{Br}\gamma$ emission (see Sect.5), as expected if the UV continuum were heating dust locally. The only plausible explanation is that the H–K color excess is due to reddening.

There is a moderate large-scale extinction gradient across the minor axis of the galactic disk (i.e. from the NW to the SE), resulting from the greater effectiveness of dust absorption on the near side of the galactic disk (fewer bulge stars in front of us and more bulge stars behind the dusty disk). However, the most prominent feature of the “extinction map” in Fig. 1b is the L-shaped feature ex-

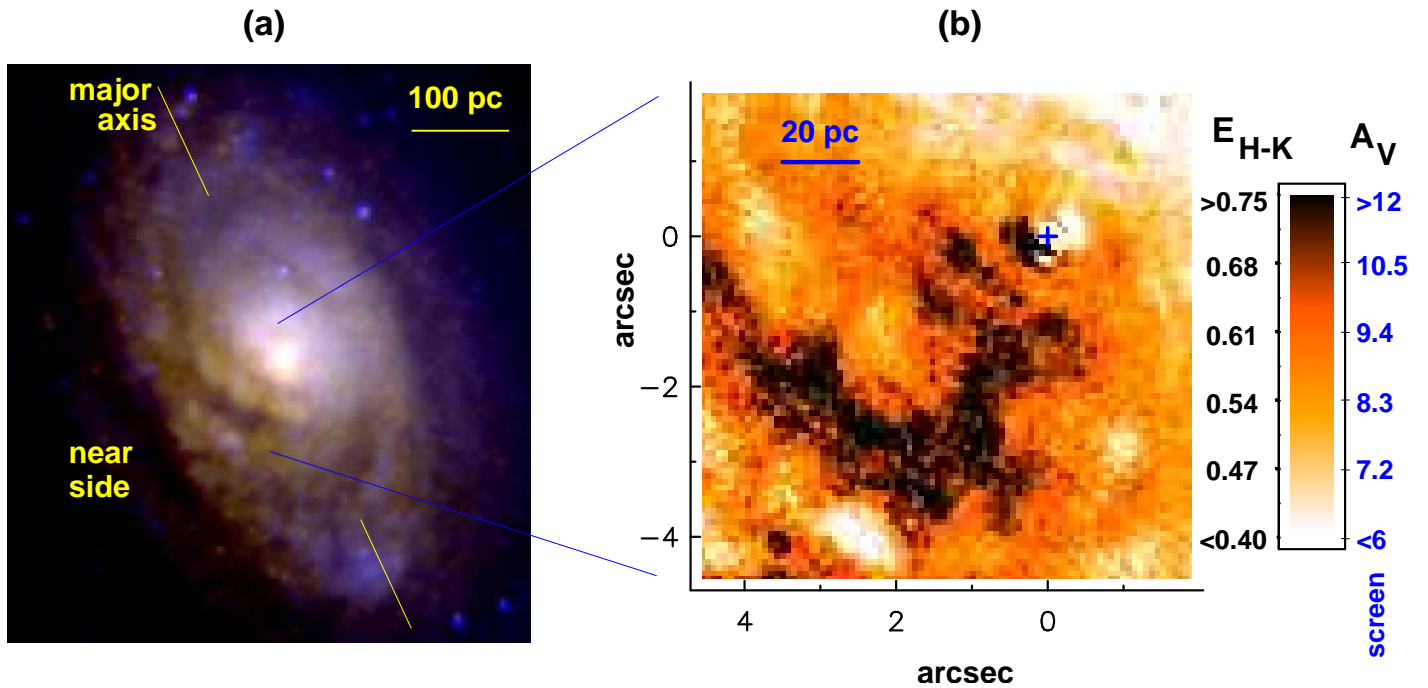


FIG. 1.— *a*) True color image of the central region of the Circinus galaxy obtained by combining HST images at $0.606 \mu\text{m}$ (WFPC2-F606W, blue), at $1.66 \mu\text{m}$ (NIC3-F166N, green) and at $2.0 \mu\text{m}$ (NIC3-F200N, red). *b*) H-K color map of the nuclear region constructed with the NIC2-F160W (\sim H band) and NIC2-F222M (\sim K band) images. The nuclear PSF was subtracted in both filters before producing the color map. The right hand side bar converts the color code into H-K color excess and into visual extinction in the case of a foreground screen model.

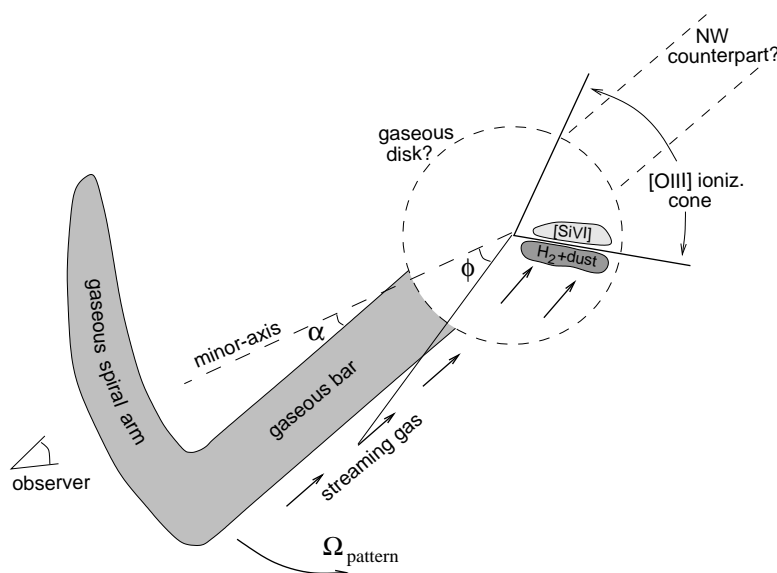


FIG. 2.— Schematic drawing of the geometry of the various components within the central few 100 pc of Circinus.

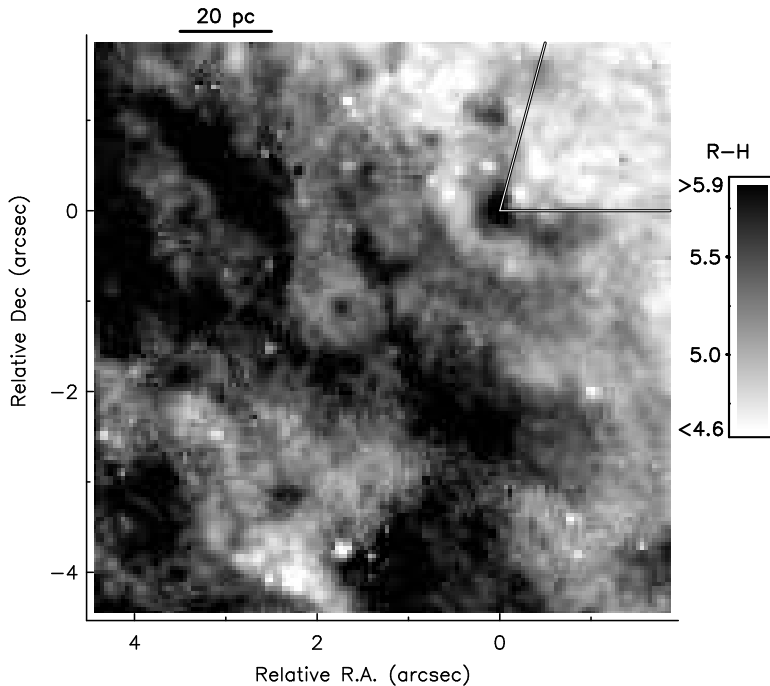


FIG. 3.— R-H color map obtained by means of the WFPC2-F606W image and the NIC2-F160W image. The straight lines indicate the orientation of the light cone observed in [OIII].

tending from the nucleus to the south-east⁵: we believe that the section of this feature elongated radially to the south is tracing the near side of a nuclear gaseous-dusty bar. The linear projected (half) size is about 50 pc. The southern end of the dusty bar tilts by about 90 degrees to the east, in a tightly wound spiral arm-like feature (see also Fig. 1a); this morphology is similar to that observed in stellar bars on larger scales, but in a gaseous version. A stellar counterpart is not present even in the K band image, where the extinction is reduced, suggesting the bar is purely gaseous.

An alternative explanation of the radial dust lane could be a warped disk (eg. Quillen et al. 1993). However, as discussed in the next section, the velocity field of the molecular gas strongly deviates from circular motion, ruling out this interpretation.

The northern extremity of the gaseous bar ends in a dusty feature that resembles a circumnuclear disk, about 20 pc in radius. Only the near side of this disk-like feature is clearly delineated, possibly as a consequence its being seen in absorption (as for the bar) and therefore the contrast is expected to be much higher on the near side. According to models, the gaseous bar is expected to form a gaseous disk in its central part during the latest stages of its evolution as a consequence of cloud-cloud viscous collisions at the denser regions near the aphelia of the orbits (Wada & Habe 1992).

Fig. 2 schematically shows the geometry of the gaseous features discussed in this section along with other components discussed in the following sections. The observed angle between the line of the minor axis and the gaseous bar is $\alpha_{\text{obs}} \approx 30^\circ$, while its deprojected value is $\alpha = \tan^{-1}(\tan \alpha_{\text{obs}} \cos i) = 16^\circ$, where i is the inclination angle of the galaxy (65°). The deprojected length of the

bar is

$$L(\text{bar}) = L_{\text{obs}}(\text{bar}) \frac{\cos \alpha_{\text{obs}}}{\cos i \cdot \cos \alpha} \approx 105 \text{ pc} \quad (1)$$

We can use the H-K color excess to derive the extinction affecting the nuclear region and, in particular, the extinction introduced by the dust in the gas bar. By assuming that the intrinsic color of the stellar population is $(H-K)_0 = 0.22$, we derive the magnitude of the dust absorption affecting the stellar light. By adopting the extinction curve of He et al. (1995) and a foreground dusty screen model we obtain: $E_{H-K} = 0.065 A_V$. The color bar on the right-hand side of Fig. 1b converts the color coding of the H-K map into color excess E_{H-K} and into visual extinction according to the extreme case of a foreground dusty screen.

The foreground screen model is the most conservative assumption: given a color excess it provides the lowest A_V . In a more realistic case, dust will be partly mixed with stars. Also, a fraction of stars will also be present in foreground and their contribution is more important in the most obscured regions. The latter effect is dominant in the optical, indeed the heavy dust obscuration affecting the nuclear region is so high that these regions are essentially invisible at optical wavelengths. This effect becomes more obvious in Fig. 3 where we have constructed an R-H color map of the central region of Circinus with the WFPC2 F606W and the NIC2 F160W images. This map shows a very irregular structure and no evidence for the dusty bar detected in the H-K color map. This is a consequence of the heavy obscuration that completely absorbs the optical light and that, therefore, makes the R band image completely dominated by the foreground stars and more affected by small variations in the extinction. We tried to describe these effects with a simple but more quantita-

⁵Evidence for this structure, though at lower angular resolution, is observed also in the H-K color map presented in Maiolino et al. (1998).

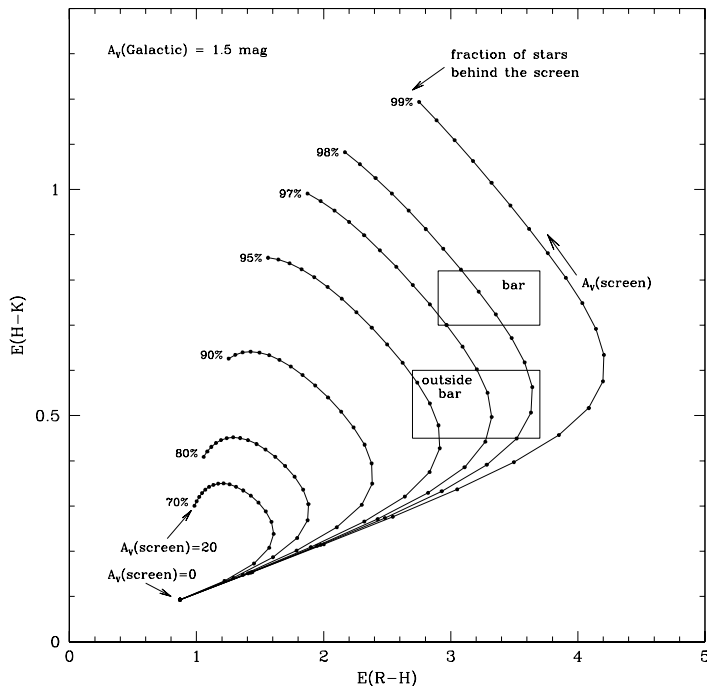


FIG. 4.— Expected H–K and R–H color excess in the case of a dusty screen that obscures only a fraction of the stars (the whole system is then obscured by a Galactic extinction $A_V = 1.5$ mag). Each curve gives the color excess for an increasing absorption of the screen and for a given fraction of stars behind the dusty screen. Points along each curve are separated by $\Delta A_V = 1$, and the total extinction ranges from $A_V = 0$ to $A_V = 20$. The two boxes show the range of color excess along the gas bar and outside the bar.

tive model. We make the simplistic assumption that the distribution of dust and stars can be described by a homogeneous dusty screen that hides most of the stars while a small fraction of the stars is in the foreground. This simple model was used for other heavily obscured systems (eg. McLeod et al. 1993). The whole system is then obscured by a Galactic absorption $A_V(\text{Gal}) = 1.5$ mag (Freeman et al. 1977). In this model, the color excess between two wavebands at λ_1 and at λ_2 is given by

$$E_{\lambda_1-\lambda_2} = A_{\lambda_1}(\text{Gal}) - A_{\lambda_2}(\text{Gal}) + 2.5 \log \left[\frac{1 - f_{\text{hid}}(1 - 10^{-A_{\lambda_1}(\text{scr})/2.5})}{1 - f_{\text{hid}}(1 - 10^{-A_{\lambda_2}(\text{scr})/2.5})} \right] \quad (2)$$

where f_{hid} is the fraction of stars that are hidden by the dust screen, while $A(\text{Gal})$ and $A(\text{scr})$ are the Galactic and screen absorption respectively. Fig. 4 shows the expected H–K and R–H color excess as a function of $A_V(\text{scr})$ and for different fraction of stars behind the dusty screen. Two boxes indicate the color excesses measured along and outside the gas bar. The R–H color excess is the more uncertain quantity, not only because of the observed large dispersion (Fig. 3), but also because the unabsorbed, intrinsic R–H color is not well defined. We adopted $(R - H)_0 \simeq 2.3$ from an average of the colors of Sc spirals in Frogel (1985) and in Fukugita et al. (1995), but the scatter is very large. Fig. 4 shows that $\sim 98\%$ of the stars behind the dusty screen and a screen absorption of $A_V(\text{scr}) \simeq 12$ mag can explain the color excess observed along the gas bar. The regions next to the bar can be explained by a fraction of stars behind the screen of $\sim 97\%$ and an extinction reduced to $A_V(\text{scr}) \simeq 7.5$ mag.

If we adopt an intermediate model with $f_{\text{hid}} = 97.5\%$ for both the regions along and outside the gas bar, then we expect the following differences in terms of surface brightness

(mag/arcsec²) between the two zones: $\Delta\mu_R \approx 0.27 \pm 0.2$, $\Delta\mu_H \approx 0.65 \pm 0.35$ and $\Delta\mu_K \approx 0.4 \pm 0.2$. Observationally, we obtain: $\Delta\mu_R \approx 0.37 \pm 0.22$, $\Delta\mu_H \approx 0.30 \pm 0.10$ and $\Delta\mu_K \approx 0.15 \pm 0.04$. There is a fair agreement between observations and expected values that, however, is worse at longer wavelength. This probably indicates that our model is too simplistic and, in particular, that a fraction of star is probably mixed with the dusty screen and that the dusty screen is not completely homogeneous as assumed.

The visual extinction along the bar is about 12 magnitudes. If we assume the Galactic gas-to-dust ratio ($N_H = 2.2 \times 10^{21} A_V \text{ cm}^{-2}$), then the column density is $N_H \approx 2 \times 10^{22} \text{ cm}^{-2}$. Note, however, that for active galaxies the standard conversion factor very likely underestimates the real N_H , as discussed in Maiolino et al. (1999b).

3.2. Evidence for streaming motions

The kinematics of the gas in the presence of a barred potential has been studied by several authors (Athanasoula 1992, Piner et al. 1995, Wada & Habe 1995, Friedli & Benz 1993). Either gravitational torques due to the offset of the gas lanes with respect to the bar axis, or shocks along the gaseous lane, cause the gas on the leading side of the bar to lose its angular momentum and, as a consequence, to flow toward the nucleus. These motions translate into a strong velocity gradient across the leading side of the bar that should be observed in the Doppler maps of the emission lines. Such a velocity pattern has been observed in several large scale stellar bars (eg. Laine et al. 1999, Regan et al. 1997). We have used our integral field near IR data to trace the velocity field of the molecular gas with

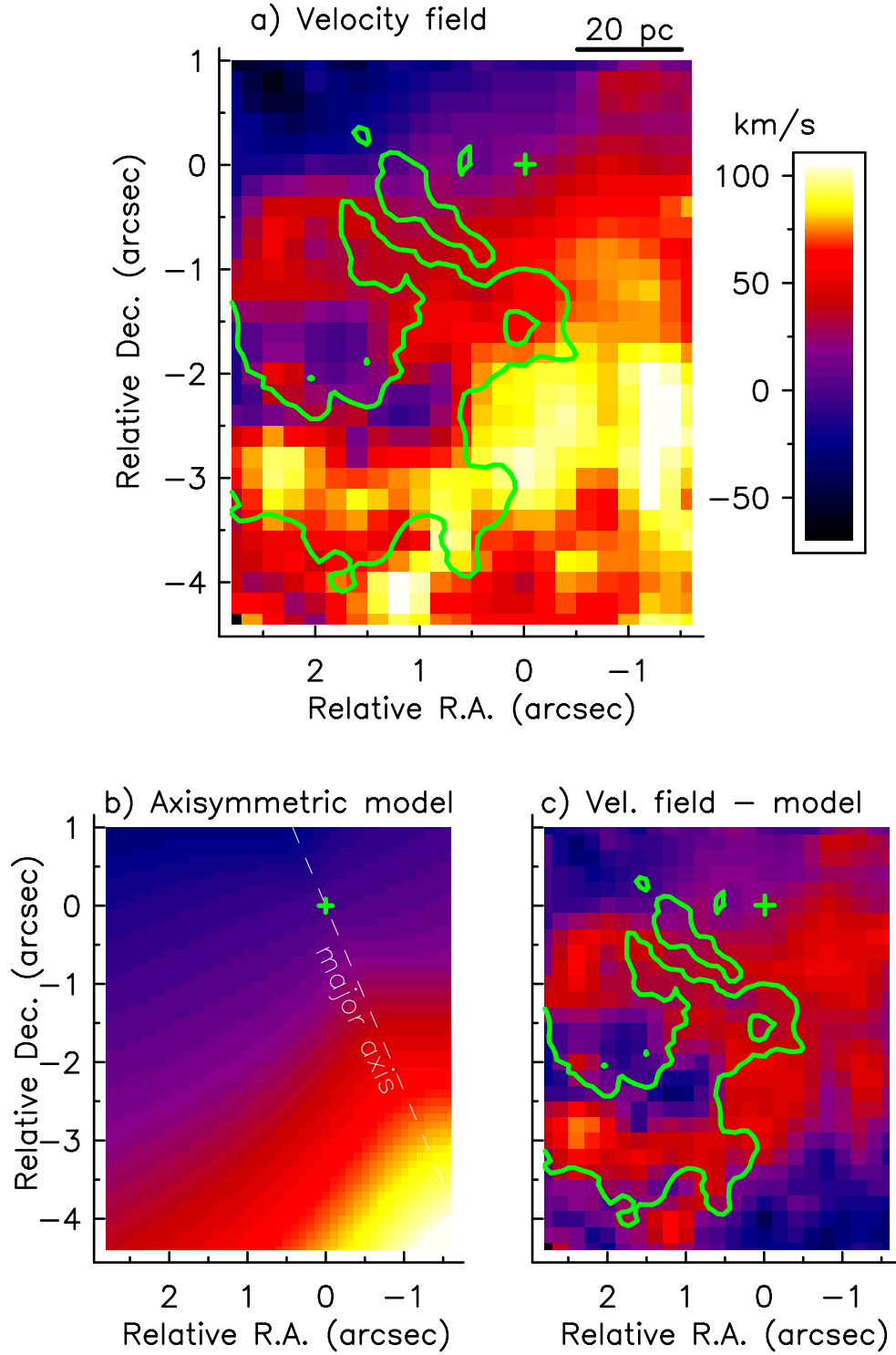


FIG. 5.— *Color image*: velocity (Doppler) field of the molecular gas as traced by the H_2 S(1)(1-0) emission line at $2.12 \mu\text{m}$, obtained by means of the 3D data. *Green line*: one of the H-K contours indicating the location of the dusty bar. *b*) Model of the velocity field expected in the case of absence of a barred potential (i.e. axisymmetric rotation). *c*) Difference between the observed velocity field and the axisymmetric model in *b*.

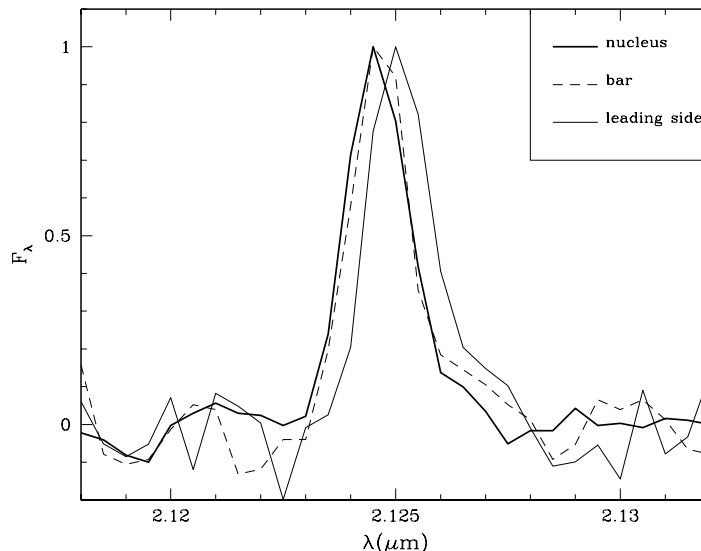


FIG. 6.— Profile of the $\text{H}_2(1-0)2.12\mu\text{m}$ line on the nucleus, on the gas bar ($1''$ to the east and $2.2''$ to the south of the nucleus) and on the leading side ($0.3''$ to the west and $2.5''$ to the south). The extraction radius is $1''$.

the H_2 $\text{S}(1)(1-0)$ emission line at $2.12\mu\text{m}$. Fig. 5 gives the radial velocity of the molecular gas as traced by the centroid of the H_2 line and relative to the systemic velocity of 438 km/s , derived from the 21 cm line⁶. The color bar on the right-hand side of Fig. 5 translates the color coding into the radial velocity corresponding to the shift of the line. The green curve is one of the contours of the H-K map indicating the location of the gas bar. We excluded from our velocity mapping most of the regions that were poorly sampled by the dithering (i.e. with low effective integration time) since the signal to noise on the H_2 line is too low in most of these regions.

The most prominent features of this map are the strong velocity gradient and the highly redshifted gas along the leading side of the bar, indicating gas streaming toward the nucleus in agreement with the model predictions. This velocity field not only supports the reality of the gaseous bar, but directly shows inflow motions that probably contribute to the feeding of the active nucleus.

The gas velocity pattern is similar to the what observed in large scale stellar bars. Here the main difference, besides the much reduced size, is that the mass that exerts the torques generating the gas inflow is not dominated by the stars but by the gas.

To show that the redshifted gas along the leading side is not due to noise or statistical fluctuations, Fig. 6 shows the spectrum of the H_2 line along the leading side and compares it with the spectrum of the nucleus and with the spectrum of the central part of the bar (see figure caption for details). The line peak was normalized to one. The signal-to-noise on the line is high, and the shift of the line along the leading side is clearly systemic and not due to noise fluctuations.

The streaming motions become obvious when compared to the rotational velocity field expected to dominate the kinematics in the absence of a barred potential. We have

modeled the velocity pattern expected if the gravitational field is dominated by the stars that are traced by the K-band light (corrected for extinction), characterized by an average mass-to-light ratio $M/L_K \approx 2.5 M_\odot/L_\odot$ (Maiolino et al. 1998). The resulting velocity field is shown in Fig. 5b. In the outer regions ($> 100\text{ pc}$, where the bar should not play a role), it is in agreement with the observed velocity field (Maiolino et al. 1998, Storchi-Bergman et al. 1999). Fig. 5c shows the deviations of the observed velocity field relative to the rotational field expected in the axisymmetric case: the most obvious deviation is the strip of redshifted gas along the leading side of the gaseous bar, in agreement with model predictions and as observed in large scale stellar bars.

The velocity maps (both Figs. 5 a and c) also show a strong gradient along the dusty spiral arm that extends from the southern end of the bar to the east, also as predicted by models (see eg. Piner et al. 1995). There is also a region of redshifted gas to the east of the nucleus; some numerical simulations show the formation of a velocity gradient in this region (Athanasoula 1992, Piner et al. 1995): indeed this region is located about at one of the apheia of the bar, where a significant population of x_2 orbits can reduce the average velocity of the gas with respect to the circular axisymmetric motions.

The largest velocities of the streaming gas along the bar are expected to occur close to the center (near the perihelia), as is actually observed in large scale stellar bars. Such high velocity gas is also observed in the nuclear region of Circinus. In Fig. 7a the green contour is a channel map of the H_2 emission with velocity Doppler shift between $+200$ and $+260\text{ km/s}$, while the color image is the [SiVI] map that will be discussed in Sect. 4. There is clear evidence for highly redshifted gas at the end of the gaseous bar, close to the nucleus. In this region the deprojected velocity is about 300 km/s .

⁶The nuclear velocity of H_2 , as well as of other low ionization lines and of the stellar features (Fig.6 of Maiolino et al. 1998), shows a small redshift of about 20 km/s . This redshift was also observed in high resolution echelle spectroscopic observations (Oliva, private communication). This redshift might arise from the definition of the velocity for the 21 cm line. Otherwise, it might reflect small, systemic differences between the central region and the outer parts of the galaxy.

The velocity field of the central region (20–40 pc) is however dominated by a normal rotation pattern: here the isovelocity lines are parallel to the minor axis. This nuclear rotation might be associated with the disk-like feature observed in the H–K color map.

Summarizing, the molecular gas velocity field shows clear non-circular motions. The general behavior of the kinematics can be ascribed to streaming motions due to the gaseous bar. Obviously, we cannot rule out more complex situations, especially concerning irregularities and details of the velocity field. Higher angular and spectral resolution and a more detailed modelling of the gas kinematics in this region are required to further support our findings and/or provide new insights on the details of the gas dynamics.

4. THE INNERMOST REGION OF THE IONIZATION CONES

4.1. *The 10 pc scale*

The gas inflow through the bar not only brings material close to the nuclear black hole, but probably plays an important role also in other phenomena of the nuclear activity such as the ionization cones and the star formation. Fig. 7a shows the NICMOS map of the [SiVI] coronal emission line. The [SiVI] emission extends in the ionization cone traced by the [OIII] optical images (Marconi et al. 1994a), as indicated by the dashed lines. The presence of [SiVI] emission also on the eastern side of the nucleus provides evidence for a counter-cone, whose existence was also inferred from the larger scale radio maps (Elmouttie et al. 1995, 1998c). The foreground extinction due to the nuclear dusty feature (disk?) is very likely responsible for the reduced [SiVI] brightness of the counter cone. If the nuclear dusty feature produces an extinction of $A_V \sim 9$ mag (as inferred from Fig. 1b), this would imply $A_{[\text{SiVI}]} \sim 1.1$, fully accounting for the brightness difference between the two cones, about a factor of 3.

The [SiVI] emission is not azimuthally uniform within the (NW) ionization cone; the southern edge appears much brighter than the rest. It is likely that the gas transported by the bar enters the ionization cone in this region. This interpretation is supported by the distribution of the molecular gas shown in Figs. 7 *a* and *b*, where we report the 3D maps of the integrated $\text{H}_2\text{S}(1)(1-0)$ emission line and the highest velocity component of the gas traced by this line. These maps show the presence of large quantities of gas just south of the ionization cone, that is flowing at high velocities towards the southern edge of the ionization cone. Next to the edge of the cone the H_2 emission is highest because here the molecular gas is more exposed to the nuclear radiation, but also because the gas density is high and the H_2 has not had time to dissociate fully. Indeed, the R–H color map (Fig. 3) clearly shows a prominent dust lane extending along the southern edge of the ionization cone, coincident with the H_2 emission. As soon as these dense clouds enter the ionization cone they are ionized and emit the [SiVI] line, but also Pa α (Fig. 7c); this gas is very dense and therefore the ionized gas emission is very high. Another dust lane in Fig. 3 traces the northern edge of the ionization cone.

Another possible explanation of the emission line and dust lane morphology is that these features are simply the

effect of the orientation of the ionization cone with respect the nuclear part of the galactic gaseous disk, which might be warped on these small scales (Quillen et al. 1999, Mulchaey et al. 1996, Schreier et al. 1998). The brighter part of the ionization cone might correspond to the region closer to denser gas of such nuclear disk. The only difficulty with this model is to obtain a projected velocity in excess of 200 km/s, as observed in Fig. 7a.

As shown in Figs. 7 *a* and *b* the molecular clouds enter the ionization cone very close (~ 10 pc) to the nucleus, where the radiation pressure is very high. As discussed in Binette (1998) the radiative acceleration is given by $a_{\text{rad}} \approx (n/1200\text{cm}^{-3})(U_0/0.125)(3.1 \times 10^{-7} + 5.8 \times 10^{-6}\mu_{\text{D}})$ [cm s^{-2}], where n is the gas numerical density, U_0 is the ionization parameter and μ_{D} the dust content with respect to the solar value. The density of the coronal line region was estimated to be about 5000 cm^{-3} based on the infrared [NeV] doublet (Moorwood et al. 1996). Oliva et al. (1999) determined U_0 for a single cloud in the ionization cone; we scaled this value to the distance of 10 pc and to the density of 5000 cm^{-3} , i.e. $U_0 \approx 1$. With these values $a_{\text{rad}} \approx 3 \times 10^{-5} \text{ cm s}^{-2}$ for a dust content of $\mu_{\text{D}} = 0.1$. Maiolino et al. (1998) set an upper limit to the mass of a nuclear black hole in Circinus of $4 \times 10^6 M_{\odot}$. The gravitational pull at a distance of 10 pc is estimated to be $4 \times 10^{-6} \text{ cm s}^{-2}$, i.e. about one order of magnitude lower than the radiative acceleration. Therefore, these clouds just driven into the ionization cone will be pushed outward to form an outflowing component of the Coronal Line Region and of the NLR. This outward acceleration of the coronal line clouds, as well as the tendency of the clouds to be ablated under the strong radiation pressure (Mathews 1986), is probably responsible for the lower emissivity of the [SiVI] line in the northern part of the cone. The denser clouds injected into the cone will survive ablation and will be accelerated like “bullets”. Veilleux & Bland-Hawthorn (1997) discovered the presence of supersonically ejected clouds ($V_{\text{eject}} > 100 \text{ km s}^{-1}$) in the Circinus NLR, which they ascribe to some explosive nuclear event. We claim that such ejected “bullets” are the result of the radiative acceleration of the dense clouds that have been driven into the ionization cone by the gaseous bar or by the nuclear disk. As suggested by Binette (1998), the radiation pressure-driven outflow would explain the blueshift of the coronal lines observed in Circinus (Oliva et al. 1994) and in other Seyfert galaxies (Penston et al. 1984), as well as the dependence of the blueward asymmetry of the narrow lines on the ionization potential and on critical density (DeRobertis & Shaw 1990, Dahari & De Robertis 1988, Whittle 1992, Heckman et al. 1981). A potential problem of the “outflow model” would be that new gas must be continuously supplied to the inner part of the cone to replace the outflowing gas. The gas flow provided by the gaseous bar or by the nuclear disk could to be the mechanism responsible for feeding the inner part of the ionization cone (a more quantitative discussion is given in sect.6.4).

On the other hand, a large fraction of the gas in the outer regions of the NLR (100 pc scale), characterized by lower ionization emission species, is probably part of the normal galaxy disk illuminated by the nuclear source. Indeed, the kinematics of the outer parts of the ionization cone are also characterized by a rotational component (Elmouttie et al. 1998b, Veilleux & Bland-Hawthorn 1997).

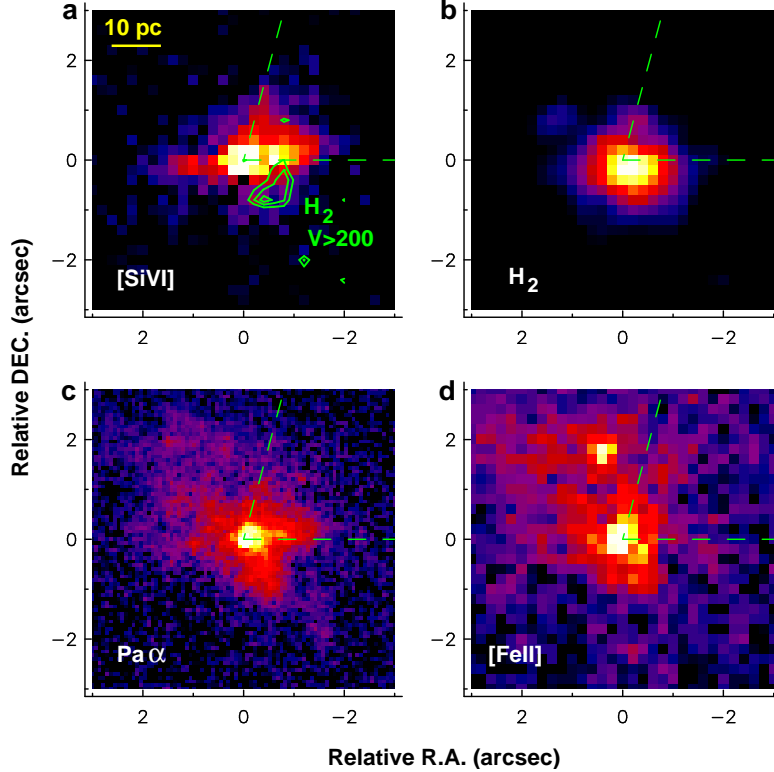


FIG. 7.— *a*) NICMOS map of the [SiVI] 1.96 μm line (color) along with the 3D channel map of the H_2 2.12 μm line with the highest velocity component ($200 < V < 260$ km/s). *b*) 3D map of the integrated emission of the H_2 2.12 μm emission line. *c*) NICMOS map of the Pa α emission line. *d*) NICMOS map of the [FeII] 1.64 μm emission line. The green dashed lines indicate the orientation of the light cone observed in [OIII].

4.2. The parsec scale

Another interesting feature of the emission line maps in Fig. 7 is that both the [SiVI] and [FeII] lines peak on the nucleus: although both show extended emission, a large fraction of the integrated flux ($\sim 70\%$ for [SiVI]) comes from an unresolved source coincident with the 2.2 μm continuum peak, i.e. the location of the active nucleus. The shift of the [SiVI] peak observed in the lower resolution data of Maiolino et al. (1998) was due to a blend of the nuclear component with the extended component to the west. Although, a fraction of the coronal lines might be excited by shocks, most of the coronal line emission must be ascribed to photoionization (Oliva 1997). However, according to photoionization models, the [SiVI] is expected to peak at the outer edge of the He^{+2} Strömgen sphere, while the [FeII] should peak right after the H^+ Strömgen sphere. With the luminosity of Circinus and a density of 10^4 cm^{-3} (i.e. even higher than what is estimated through the [NeV] infrared lines) Oliva et al. (1999) derived that the [SiVI] should peak at about 30 pc from the nucleus. The [FeII] emission should peak even further out. There are a few possible explanations of this inconsistency:

1. As suggested by Oliva et al. (1999), the ionized clouds are dusty. The ionization parameter in these regions is very high ($U \sim 1$) and, therefore, the dust competes with the gas in absorbing UV photons thus reducing significantly the size of the Strömgen

spheres. This might be the case for the [FeII] emission. Yet the clouds responsible for the emission of most coronal lines (including [SiVI]) appear characterized by little dust content⁷ and, therefore, dust probably plays a minor role in the ionization structure of these clouds.

2. Another possibility is that the gas that emits most of the coronal lines is significantly denser, shrinking the size of the He^{+2} sphere. More specifically $R(\text{He}^{+2}) \propto N_e^{-2/3}$. Reducing the radius of the [SiVI] emitting shell from 30 pc to less than 10 pc (which would make the emission unresolved) would require an electron density larger by a factor of 5, i.e. $N_e = 5 \times 10^4 \text{ cm}^{-3}$. However, this density is one order of magnitude higher than what measured from the [NeV] doublet (Moorwood et al. 1996). Also, the thickness of the [SiVI] emitting shell (Marconi et al. 1994b), relative to $R(\text{He}^{+2})$, is inversely proportional to N_e and, therefore, the [SiVI] line would be significantly fainter than other coronal lines that form inside the He^{+2} sphere, i.e. higher ionization species. This line of reasoning applies as long as the ionization structure has a quasi-spherical geometry (Oliva 1997). If a nuclear population of very dense clouds exists, more specifically with $N_e > 10^5 \text{ cm}^{-2}$ (but still lower than the critical density of $\sim 10^8 \text{ cm}^{-2}$), then the geometry of the ionization structure is quasi-plane parallel ($R > 10 \Delta R$) and the region of [SiVI] emission extends over the

⁷Oliva et al. show that very likely most of the Fe is in the gaseous form in the coronal line region.

whole He^{+2} Strömgen region. This would solve the problem of the ratio between [SiVI] and the higher ionization coronal lines, but the lower density measured with the [NeV] lines remains an issue.

3. Increasing the filling factor would also reduce the size of the emission region ($R(\text{He}^{+2}) \propto f^{-1/3}$), but this would also affect the coronal line ratios similarly to the change in density discussed above.
4. A final, interesting possibility is that the nuclear UV emission is intrinsically non-isotropic (Oliva et al. 1999), as is expected to be the case if the emission arises from an optically thick accretion disk. In the latter case the azimuthal clouds are illuminated by a flux that is significantly lower than the face-on flux ($L_{\text{AGN}} \propto (\cos\theta)^{-1}$, Laor & Netzer 1989). The He^{+2} Strömgen radius of the azimuthally distributed gas would be much smaller than that estimated above and could very well appear point like at our resolution.

5. NUCLEAR STAR FORMATION

The $\text{Pa}\alpha$ and the [FeII] emission appear much more diffuse and extended⁸ than the [SiVI]. Both emission lines extend well outside the ionization cone and preferentially along the major axis of the galaxy, although the $\text{Pa}\alpha$ also has a component in the ionization cone similar to that observed in the [SiVI] map. Very likely the diffuse/extended emission traces moderate star forming activity occurring within the central 50 pc as a result of the large amount of molecular gas driven into this region by the gaseous bar. The $\text{Pa}\alpha$ emission traces the UV radiation from young OB stars. Maiolino et al. (1998) used the circumnuclear $\text{Br}\gamma$ emission and the mass-to-light ratio to model the star formation history, and infer that the nuclear stellar population has an age of about 10^8 yr.

Fig. 7c shows that the star formation history of the nuclear region is probably more complex. The $\text{Pa}\alpha$ map shows the presence of knots and non-axisymmetric emission: a chain of three HII region is present at about 20 pc to the north-east of the nucleus, while a burst of star formation is present to the south-west, right at the nuclear end of the leading side of the gaseous bar. These are the locations of the apelia of the bar, where orbit crowding is indeed expected to enhance the star formation (Wada and Habe 1992). There is no evidence for star forming activity along the bar. Although large concentrations of gas are expected along the leading side of the bar, star formation might be inhibited by the strong shear forces (Elmegreen 1979, Kenney & Lord 1991).

The diffuse [FeII] emission probably traces gas shocked by supernova explosions. A bright [FeII] knot, about 30 pc to the north of the nucleus very likely traces a single young supernova remnant. The [FeII] knot is unresolved (i.e. $R < 4$ pc), thus implying that the SNR must be younger than about 100 yr. There is also a prominent [FeII] extension to the south of the nucleus, slightly offset with respect to the $\text{Pa}\alpha$ emission; shocks due to the gas streaming from the gaseous bar might also play a role in this region.

6. DISCUSSION

6.1. Plausibility of the gas bar and open issues

Although the presence of a nuclear gas bar appears convincing both from the morphological and the kinematical points of view, we can check whether the physical conditions of the gas meet the requirements necessary to develop the gravitational instabilities that should form a bar. According to models, a gaseous bar should form when the mass of the gaseous nuclear disk is larger than 10 (Wada & Habe 1992) to 20% (Shlosman et al. 1989), of the dynamical mass. CO(2–1) millimetric data (Aalto et al. 1995, Johansson et al. 1991) indicate that the gas mass enclosed within the central 400 pc is about $6 \times 10^8 M_{\odot}$, if the Galactic conversion factor is assumed (Kenney & Young 1989). Based on the kinematical information provided by Maiolino et al. (1998) we estimate that the dynamical mass inside the same region is about $1.2 \times 10^9 M_{\odot}$, i.e. only a factor of two higher than the mass in molecular gas. Therefore, the physical conditions of the gas in the nuclear region are indeed appropriate for the formation of a gaseous bar (although this argument is weakened if the conversion from CO to gas mass is less than the standard Galactic value, as sometimes appears to be the case in extreme starbursts).

In the H–K color map (Fig. 1b) only one side of the gaseous bar is observed; the north–west counterpart is not seen. One possible explanation is that the other side of the gaseous bar is present but it is not observed in the extinction map because the contrast of absorption features is much lower on the far side of the disk (more foreground stars and less stars behind). Otherwise the north-west side of the bar might be intrinsically weaker or even absent. Since gaseous bars are formed via gravitational instabilities, they are expected to be highly inhomogeneous and possibly asymmetric, especially on such small scales.

Another important issue to address is whether these gaseous bars are rare cases or they could be a fuelling mechanism common to most active galaxies as claimed by Shlosman et al. (1989). If the latter is the case then the question is why such nuclear gaseous bars were detected only in a few active nuclei (Mulchaey & Regan 1999, Henkel et al. 1991, Ishizuki et al. 1990), or none if we only consider nuclear bars as small as the one in Circinus. These gaseous bars can be identified from molecular gas emission (eg. CO millimetric maps) and/or through dust absorption traced by the color maps, as we have done in this work. Circinus is closest Seyfert 2 known and the projected angular size of the gaseous bar is 2 arcsec. Most of the other Seyfert galaxies are further away and, therefore, a nuclear gaseous bar with similar size would have a much smaller angular size, which would make it hard to detect. The average distance of the Seyfert galaxies in the sample of Maiolino & Rieke (1995) is 32 Mpc and the projected size of the nuclear gaseous bar would be a few tenths of arcsecond, unresolved even at the NICMOS resolution (at $2 \mu\text{m}$) and at the resolution of the current millimetric interferometers. Also, we emphasize that the color map technique to search for gaseous bars works as long as infrared filters are used. In these heavily obscured nuclei the optical images sample only the outer (foreground) parts of the nuclear region and therefore do not provide the required information even if compared with an infrared image to

⁸The [FeII] morphology observed in our NICMOS image is consistent with the lower resolution map obtained by Davies et al. (1999).

obtain a color map. Indeed, as shown in Fig. 3 and as discussed in sect.3.1, the R–H color map of Circinus does not show evidence for the dusty bar detected in the H–K color map. This result may partly explain the shortage of gaseous bars in Regan & Muchaey (1999), a work which included images taken through the above filters of a sample of Seyferts. Summarizing, whether nuclear gas bars are a common feature in Seyfert galaxies or not remains an open question, since such structures might have been missed in previous studies both because of limited angular resolution and/or inappropriate techniques.

6.2. Fuelling the active nucleus

As discussed in Athanassoula (1992) and Regan et al. (1997), probably only a small fraction of the streaming gas does actually result in an inflow (10%–30%). We can estimate the streaming flux of the gas along the leading edge of the nuclear bar in Circinus and compare it with the inflow requirements to feed the active nucleus. The gas streaming flow along the leading edge of the bar (an upper limit to the real inflow rate) is given by:

$$\dot{M}_{\text{stream}} = N_{\text{H}} w V_{\text{stream}} m_{\text{p}} \quad (3)$$

where w is the width of the streaming gas lane (~ 20 pc), m_{p} is the proton mass, V_{stream} is the streaming gas velocity along the leading edge of the gaseous bar and N_{H} the gas column density in the same region ($\sim 2 \times 10^{22} \text{cm}^{-2}$, sect.3.1). To determine V_{stream} we have to correct the observed redshifted velocity for various projection effects and for the contribution due to the pattern circular motion, as illustrated in Fig. 2. More specifically:

$$V_{\text{stream}} = \frac{V_{\text{D}}(\text{obs})/\cos i - V_{\text{pattern}} \sin \phi}{\cos \alpha} \quad (4)$$

where V_{D} is the Doppler velocity shift observed along the leading edge of the bar, ϕ is the deprojected angle between the galaxy minor axis⁹ and the line connecting the nucleus to the specific point along the leading edge of the bar where the redshifted gas is observed (see Fig. 2), V_{pattern} is the velocity component due to pattern speed at the same location, while i and α were defined in Sect.3.1. The outer edge of the gaseous bar is located at about 160 pc from the nucleus, probably the location of the corotation radius. At this distance the rotational velocity is 150 km/s (deprojected for inclination, Maiolino et al. 1998), thus giving a pattern speed of $\Omega_{\text{pattern}} = 0.92 \text{ km s}^{-1} \text{ pc}^{-1}$. If we consider the streaming gas located at about the mid-point of the gaseous bar, then the deprojected distance from the nucleus is about 90 pc, hence $V_{\text{pattern}} = 83 \text{ km/s}$, and $\phi = 25^\circ$. The contribution from the circular pattern velocity ($V_{\text{pattern}} \sin \phi$) is very low, as expected since the bar is oriented almost along the line of sight. With these values we estimate $V_{\text{stream}} = 83 \text{ km/s}$, hence from Eq. 6.2 we derive a streaming flow rate of $\dot{M}_{\text{stream}} \approx 0.25 M_{\odot} \text{yr}^{-1}$.

The luminosity of the active nucleus is about $2 \times 10^{40} L_{\odot}$, or lower if the nuclear emission is intrinsically anisotropic (Oliva et al. 1999), thus implying an accretion rate of

$$\dot{M}_{\text{AGN}} = L_{\text{AGN}}/c^2 \epsilon \approx 10^{-2} M_{\odot} \text{yr}^{-1} \quad (5)$$

⁹More specifically the direction orthogonal to the line of nodes and on the plane of the galaxy.

(where we assumed a radiation efficiency $\epsilon = 0.1$). The streaming flow estimated above is 25 times higher than the AGN accretion rate. Therefore even if only 10% of the streaming gas actually flows into the nucleus, this will provide 2.5 times as much fuel as required to power the activity.

6.3. Fuelling the nuclear star formation

As discussed above, Pa α emission traces regions of recent star formation, while the smoother near-IR continuum emission traces the older stellar population evolved from past bursts. We can estimate the current star formation rate from the Pa α emission due to stellar activity integrated in the nuclear region. We subtracted the contribution to the Pa α emission due to the active nucleus by normalizing the [SiVI] map to the Pa α on the nucleus; this is actually a conservative subtraction of the AGN Pa α flux, since a fraction of the unresolved nuclear Pa α emission, as well as part of the Pa α emission within the cone, might be due to star formation as well. The flux of the AGN-subtracted Pa α integrated within a radius of 30 pc ($= 1''.5$) is $1.2 \times 10^{-13} \text{ erg s}^{-1} \text{ cm}^{-2}$. If we assume that the extinction derived from the H–K color map in Fig. 1 also applies to the nebular emission, then on average $A_{\text{V}} \sim 9$ mag, hence $A_{\text{Pa}\alpha} \sim 1.3$ mag. Therefore the extinction corrected Pa α flux is $4 \times 10^{-13} \text{ erg s}^{-1} \text{ cm}^{-2}$. At the distance of 4 Mpc, this flux translates into a ionizing photon flux $Q_{\text{i}} = 1.4 \times 10^{51} \text{ s}^{-1}$. We employed the stellar population synthesis code described in Sternberg & Kovo (1999) to derive the star formation rate required to produce this ionizing photon flux. By adopting a Salpeter initial mass function and an upper mass cut-off of $60 M_{\odot}$ we obtain a star formation rate of $\sim 10^{-2} M_{\odot} \text{yr}^{-1}$. This star formation rate is relatively low and similar to the accretion rate of the active nucleus. The amount of gas inflow provided by the gaseous bar (sect.6.2) can feed both the active nucleus and the star forming activity in the nuclear region.

6.4. Fuelling the ionization cone

As discussed in sect.4.1 part of the gas observed in the ionization cone is in circular motion in the galactic plane, while a fraction of the gas is outflowing, probably as a consequence of the nuclear radiation pressure. We speculated that the inflow due to the gas bar might supply to the nucleus the material that is being ejected through the ionization cone. Here we address this possibility more quantitatively. Veilleux & Bland-Hawtorn (1998) estimate the kinetic energy in the outflowing gas and in the ejected filaments to be about $K \approx 10^{52} (N_{\text{e}}/100 \text{cm}^{-2}) \text{ erg}$. By approximating with a spherical outflow, the kinetic energy can be converted into a mass outflow rate according to the formula $\dot{M}_{\text{outfl}} \approx 2K/(V_{\text{outfl}}R)$, where V_{outfl} is the (deprojected) outflow velocity and R is the average distance of the outflowing gas detected in the images. By assuming $V_{\text{outfl}} \approx 200 \text{ km/s}$ (Veilleux & Bland-Hawtorn 1998) at an average distance of about 100 pc, and by assuming an average density $N_{\text{e}} \approx 500 \text{cm}^{-3}$ (Oliva et al. 1999), we obtain $\dot{M}_{\text{outfl}} \approx 10^{-2} M_{\odot} \text{yr}^{-1}$. Although this estimated is very rough, it shows that the outflowing component of the ionization cone requires some degree of fuelling, and that the inflow due to the gas bar can account for this fuelling.

7. CONCLUSIONS

We present NICMOS/HST images and integral field near-IR spectroscopy of the nuclear region of the closest Seyfert 2 galaxy Circinus. The H–K color map shows a nuclear dust lane that extends radially. We propose that this dust lane traces a nuclear gas bar that might be responsible for feeding the active nucleus. The velocity field traced by the H₂ line at 2.12 μm shows enhanced radial motions along the leading edge of the gas bar, in agreement with model predictions. The latter finding not only supports the identification of the gaseous bar, but directly shows gas inflow motions that probably fuel the AGN. The estimated streaming flow along the leading edge of the bar is about $0.25 M_{\odot}\text{yr}^{-1}$. Probably no more than 10–30% of this flow does actually result in an inflow rate, that is however enough to fuel the active nucleus (whose accretion rate is about $10^{-2} M_{\odot}\text{yr}^{-1}$). We cannot rule out more complex situations to explain details and irregularities of the velocity field; higher resolution spectroscopic data are required to further support our findings and/or provide new insights on the details of the gas dynamics.

Nuclear gaseous bars similar to the one in Circinus might be a fuelling mechanism common to many active nuclei hosted in gas rich galaxies. Possibly, limited angular resolution and/or inappropriate techniques might be responsible for the shortage of nuclear gas bar detections in other active nuclei.

We also used the NICMOS data to study the innermost part of the Narrow Line Region and the Coronal Line Region. The coronal line [SiVI] 1.97 μm reveals the presence of a counter-cone that was not observed at optical wavelengths, very likely because of obscuration. The [SiVI] and Pa α emission is not distributed uniformly within the ionization cone but extends preferentially along the southern edge of the cone. This enhanced emission seems associated with dense gas just outside the cone, traced by the

H₂ (molecular gas emission) and R–H (dust absorption) maps. This gas is flowing towards the cone at velocities in excess of 200 km/s. We speculate that the gas streaming from the gas bar enters the ionization cone, contributing significantly to the Coronal Line Region and to the innermost part of the Narrow Line Region. This dense gas is probably accelerated by the radiation pressure producing the outflowing gas and the ejected clouds observed in the Narrow Line Region.

Besides the extended component, both the [SiVI] 1.97 μm and the [FeII] 1.64 μm emission are characterized by a nuclear intense unresolved component, while photoionization models would expect these lines to peak at a few 10 pc from the nucleus. This finding poses important constraints on the photoionization models.

Both Pa α and [FeII] emission extend over the central 60 pc and also outside the ionization cone. Most probably this extended emission traces recent star formation in the nuclear region. The Pa α extended emission is irregular and “knotty”, different than the smoother near-IR continuum. This Pa α emission probably traces recently formed HII regions, therefore pointing to a complex nuclear star formation history. We estimate an average star formation rate in the nuclear 60 pc of $\sim 10^{-2} M_{\odot}\text{yr}^{-1}$, which could be sustained by the inflow rate due to the gaseous bar.

We thank E. Oliva, A. Marconi and the referee, M.W. Regan, for useful comments. During the course of this work A.A.-H. and A.Q. were supported by the National Aeronautics and Space Administration (NASA) on grants NAG 5-3042 and GO-07869.01-96A respectively, through the University of Arizona. R.M. acknowledges the partial financial support from the Italian Space Agency (ASI) through the grant ARS-98-116/22 and from the Italian Ministry for University and Research (MURST) through the grant Cofin98-02-32.

REFERENCES

- Aalto, S., Booth, R.S., Black, J.H., & Johansson, L.E.B., 1995, *A&A*, 300, 369
 Athanassoula, E., 1992, *MNRAS*, 259, 345
 Binette, L., 1998, *MNRAS*, 294, L47
 Curran, S.J., Johansson, L.E.B., Rydbeck, G., Booth, R.S., 1998, *A&A*, 338, 863
 Dahari, O., DeRobertis, M.M., 1988, *ApJ*, 331, 727
 Davies, R.E., et al., 1998, *MNRAS*, 293, 189
 DeRobertis, M.M., Shaw, R.A., 1990, *ApJ*, 421, 348
 Elmegreen, B.G., 1979, *ApJ*, 231, 372
 Elmouttie, M., Haynes, R.F., Jones, K.L., Ehle, M., Beck, R., Wielebinski, R., 1995, *MNRAS*, 275, L53
 Elmouttie, M., Krause, M., Haynes, R.F., Jones, K.L., 1998a, *MNRAS* 300, 1119
 Elmouttie, M., et al., 1998b, *MNRAS*, 297, 49
 Elmouttie, M., Krause, M., Haynes, R.F., Jones, K.L., 1998c, *MNRAS*, 300, 1119
 Freeman, C., Karlsson, B., Lyng, G., Burrell, J.F., van Woerden, H., Goss, W.M., Mebold, U., 1977, *A&A*, 55, 445
 Friedli, D., 1999, in *The evolution of galaxies on cosmological timescales*, eds. J.E. Beckman & T.J. Mahoney, ASP Conf. Ser., in press
 Friedli, D., Benz, W., 1993, *A&A*, 268, 65
 Friedli, D., Wozniak, H., Rieke, M., Martinet, L., Bratschi, P., 1996, *A&AS* 118, 461
 Frogel, J.A., 1985, *ApJ* 298, 528
 Fukugita, M., Shimasaku, K., Ichikawa, T., 1995, *PASP* 107, 945
 González Delgado, R.M., Heckman, T., Leitherer, C., 1998, *ApJ*, 505, 174
 Greenhill, L.J., Moran, L.M., Herrnstein, J.R., 1997a, *ApJ*, 481, L23
 Greenhill, L.J., Gwinn, C.R., 1997b, *Ap&SS* 248, 261
 Greenhill, L.J., Ellingsen, S.P., Norris, R.P., Gough, R.G., Sinclair, M.W., Moran, J.M., Mushotzky, R., 1997c, *ApJ*, 474, L103
 Greenhill, L.J., Herrnstein, J.R., Ellingsen, S.P., Reynolds, J.E., Norris R.P., Moran, J.M., Booth, R.S., 1998, *AAS*, 193, 5702
 Hasinger, G., 1998, in the proceedings of the 12th Postdam Cosmology Workshop, eds. V. Muller, S. Gottloeber, J.P. Muecket, J. Wambsganss, World Scientific, p. 353
 Heckman, T.M., Miely, G.K., van Breugel, W.J.M., Butcher, H.R., 1981, *ApJ*, 247, 403
 Helfer, T.T., & Blitz, L., 1995, *ApJ*, 450, 90
 Heller, C.H., Shlosman, 1994, *ApJ*, 424, 84
 Henkel, C., Mauersberger, R., Baan, W.A., 1991, *A&A Rev*, 3, 47
 Hernquist, L., 1989, *Nat.*, 340, 687
 He, L., Whitte, D.C.B., Kilkenny, D., Spencer, J.J.H., 1995, *ApJS*, 101, 335
 Ho, L.C., Filippenko, V., Sargent, W.L.W., 1997, *ApJS*, 112, 315
 Ishizuki, S., Kawabe, R., Ishiguro, M., Okumura, S.K., Morita, K.,-I., Chikada, Y., kasuga, T., Doi, M., 1990, *Nat.*, 334, 224 shiguro
 Kenney, S., 1997, in the *Interstellar medium in galaxies*, ed. J.M., Van der Hulst, Kluwer Academic Publisher, p.33
 Kenney, J.D.P., Lord, S.D., 1991, *ApJ*, 381, 118
 Kenney, J.D.P., Young, J.S., 1989, *ApJ*, 344, 171
 Johansson, L.E.B., Aalto, S., Booth, R.S., Rydbeck, G., 1991 in *Dynamics of Disc Galaxies*, ed. B. Sundelius, Göteborg, Sweden, p.249
 Krist, J.E., & Hook, R., 1997, *TinyTim User Guide*, Version 4.4 (Baltimore: STScI)
 Jungwiert, B., Combes, F., Axon, D.J., 1997, *A&AS* 125, 479
 Laine, S., Kenney, J.D.P., Yun, M.S., Gottesman, S.T., 1999, *ApJ*, 511, 709
 Laor, A., Netzer, H., 1989, *MNRAS*, 238, 897
 Maiolino, R., Rieke, G.H., 1995, *ApJ* 454, 95

- Maiolino, R., Ruiz, M., Rieke, G.H., Papadopoulos, P., 1997, *ApJ*, 485, 552
- Maiolino, R., Krabbe, A., Thatte, N., Genzel, R., 1998, *ApJ* 493, 650
- Maiolino, R., Risaliti, G., Salvati, M., 1999a, *A&A* 341, L35
- Maiolino, R., et al., 1999b, in prep.
- Marconi, A., Moorwood, A.F.M., Origlia, L., Oliva, E., 1994a, *ESO Mess*, 78, 20
- Marconi, A., Moorwood, A.F.M., Salvati, M., & Oliva, 1994b, *A&A*, 291, 18
- Mathews, W.G., 1986, *ApJ*, 305, 187
- Matt, G., et al., 1996, *MNRAS*, 208, 253
- Matt, G., et al., 1999, *A&A*, 341, L39
- McLeod, K.K., Rieke, G.H., Rieke, M.J., Kelly, D.M., 1993, *ApJ*, 412, 111
- McLeod, B.A., 1997, in *The 1997 HST calibration workshop with a new generation of instruments*, eds. S. Casertano, R. Jedrzejewski, C.D., Keye, M., Stevens, STScI QB 500.268 C35, p. 281
- Meixner, M., Puchalsky, R., Blitz, L., Wright, M., Heckman, T., 1990, 354, 158
- Mirabel, I.F., et al., 1999, *A&A*, 341, 667
- Miyaji T., Hasinger G., Schmidt M., 1999, in *Highlights in X-ray Astronomy in Honor of Joachim Trümper's 65th Birthday*, MPE Report, (Garching:MPE), in press
- Miyoshi, M., Moran, J., Herrnstein, J., Greenhill, L., Nakai, N., Diamond, P., Inoue, M., 1995, *Nat.* 373, 127
- Moorwood, A.F.M., et al., 1996, *A&A*, 315, L109
- Mulchaey, J.S., Wilson, A.S., Tsvetanov, Z., 1996, *ApJ*, 467, 197
- Oliva, E., Salvati, M., Moorwood, A.F.M., Marconi, A., 1994, *A&A*, 288, 457
- Oliva, E., 1997, in *Emission line in active galaxies: new methods and techniques*, eds. B.M. Peterson, F.-Z. Cheng, & A.S. Wilson, ASP Conf. Ser. 113, p. 288
- Oliva, E., Marconi, A., Moorwood, A.F.M., 1999, *A&A*, 342, 87
- Penston, M.V., Fosbury, A.E., Boksenberg, Ward, M.J., Wilson, A.S., 1984, *MNRAS*, 208, 347
- Piner, B.G., Stone, J.M., Teuben, P.J., 1995, *ApJ*, 449, 508
- Quillen, A.C., Graham, J.R., Frogel, J.A., 1993, *ApJ*, 412, 550
- Quillen, A.C., Frogel, J.A., Kenney, J.D.P., Pogge, R.W., DePoy, D.L., 1995, *ApJ*, 441, 549
- Quillen, A.C., Alonso-Herrero, A., Rieke, M.J., McDonald, C., Falcke, H., 1999, *ApJ*, in press
- Regan, M.W., Vogel, S.N., Teuben P.J., 1997, *ApJ*, 482, L143
- Regan, M.W., & Mulchaey, J.S., 1999, *ApJ*, 117, 2676
- Risaliti, G., Maiolino, R., Salvati, M., 1999, *ApJ*, in press
- Schreier, E.J., et al., 1998, *ApJ* 499, L143
- Shlosman, I., Frank, J., Begelman, M.C., 1989, *Nat.*, 338, 45
- Shlosman, I., Begelman, M.C., Frank, J., 1990, *Nat.*, 345, 679
- Sternberg, A., Kovo, O., 1999, in prep
- Storchi-Bergmann, T., Winge, C., Ward, M., Wilson, A.S., 1999, *MNRAS*, in press
- Tacconi, L.J., Gallimore, J.F., Genzel, R., Schinnerer, E., Downes, D., 1997, *Ap&SS*, 248, 59
- Thatte, N., Kroker, H., Weitzel, L., Tacconi-Garman, L.E., Tecza, M., Krabbe, A., Genzel, R., 1995, *Proceedings of the SPIE*, 2475, 228
- Thatte, N., Quirrenbach A., Genzel R., Maiolino R., Tecza M., 1997, *ApJ*, 490, 650
- Veilleux, S., Bland-Hawtorn, J., 1997, *ApJ*, 479, L105
- Wada, K., Habe, A., 1992, *MNRAS*, 258, 82
- Weitzel, L., Krabbe, A., Kroker, H., Thatte, N., Tacconi-Garman, L.E., Cameron, M., Genzel, R., 1996, *A&AS*, 119, 531
- Whittle, M., 1992, *ApJS*, 79, 49
- Wozniak, H., Friedli, D., Martinet, L., Martin, P., Bratschi, P., 1995, *A&AS*, 111, 115